NeuroImage 231 (2021) 117861

Contents lists available at ScienceDirect

NeuroImage

journal homepage: www.elsevier.com/locate/neuroimage

Reliability of EEG microstate analysis at different electrode densities during propofol-induced transitions of brain states

Kexu Zhang[a,b,c], Wen Shi[d,e], Chang Wang[a,b,c], Yamin Li[d], Zhian Liu[a,b,c], Tun Liu[a,b,c,f], Jing Li[a,b,c,f], Xiangguo Yan[a,b,c], Qiang Wang[g], Zehong Cao[h,i], Gang Wang[a,b,c,*]

[a] The Key Laboratory of Biomedical Information Engineering of Ministry of Education, Institute of Biomedical Engineering, School of Life Science and Technology, Xi'an Jiaotong University, Xi'an 710049, China
[b] National Engineering Research Center for Healthcare Devices, Guangzhou 510500, China
[c] The Key Laboratory of Neuro-informatics and Rehabilitation Engineering of Ministry of Civil Affairs, Xi'an 710049, China
[d] School of Biomedical Engineering, Shanghai Jiao Tong University, Shanghai 200240, China
[e] The Key Laboratory for Biomedical Engineering of Ministry of Education, Department of Biomedical Engineering, College of Biomedical Engineering & Instrument Science, Zhejiang University, Hangzhou 310027, China
[f] Department of Anesthesiology, Honghui Hospital, Xi'an Jiaotong University, Xi'an 710054, China
[g] Department of Anesthesiology and Center for Brain Science, The First Affiliated Hospital of Xi'an Jiaotong University, Xi'an 710061, Shaanxi, China
[h] School of Information and Communication Technology, University of Tasmania, Hobart, TAS 7001, Australia
[i] STEM, University of South Australia, Adelaide, Australia

ARTICLE INFO

Keywords:
Reliability
Microstate analysis
EEG
Propofol-induced sedation
Intraclass correlation coefficient

ABSTRACT

Electroencephalogram (EEG) microstate analysis is a promising and effective spatio-temporal method that can segment signals into several quasi-stable classes, providing a great opportunity to investigate short-range and long-range neural dynamics. However, there are still many controversies in terms of reproducibility and reliability when selecting different parameters or datatypes.

In this study, five electrode configurations (91, 64, 32, 19, and 8 channels) were used to measure the reliability of microstate analysis at different electrode densities during propofol-induced sedation.

First, the microstate topography and parameters at five different electrode densities were compared in the baseline (BS) condition and the moderate sedation (MD) condition, respectively. The intraclass correlation coefficient (ICC) and coefficient of variation (CV) were introduced to quantify the consistency of the microstate parameters. Second, statistical analysis and classification between BS and MD were performed to determine whether the microstate differences between different conditions remained stable at different electrode densities, and ICC was also calculated between the different conditions to measure the consistency of the results in a single condition.

The results showed that in both the BS or MD condition, respectively, there were few significant differences in the microstate parameters among the 91-, 64-, and 32-channel configurations, with most of the differences observed between the 19- or 8-channel configurations and the other configurations. The ICC and CV data also showed that the consistency among the 91-, 64-, and 32-channel configurations was better than that among all five electrode configurations after including the 19- and 8-channel configurations. Furthermore, the significant differences between the conditions in the 91-channel configuration remained stable at the 64- and 32-channel resolutions, but disappeared at the 19- and 8-channel resolutions. In addition, the classification and ICC results showed that the microstate analysis became unreliable with fewer than 20 electrodes.

The findings of this study support the hypothesis that microstate analysis of different brain states is more reliable with higher electrode densities; the use of a small number of channels is not recommended.

1. Introduction

The extraction of reliable biomarkers is vital for the diagnosis and treatment of neuropsychiatric illnesses. As a non-invasive and low-cost imaging tool, electroencephalography (EEG) has been widely used to measure the electrical activity of the brain and detect neural dynamic changes at the millisecond time scale, providing a practical tool for potential diagnosis of neuropsychiatric diseases (Fitzgerald and Wat-

* Corresponding author at: The Key Laboratory of Biomedical Information Engineering of Ministry of Education, Institute of Biomedical Engineering, School of Life Science and Technology, Xi'an Jiaotong University, Xi'an 710049, China.
E-mail address: ggwang@xjtu.edu.cn (G. Wang).

https://doi.org/10.1016/j.neuroimage.2021.117861
Received 9 December 2020; Received in revised form 31 January 2021; Accepted 9 February 2021
Available online 13 February 2021

son, 2018; Sharmila, 2018). Many existing signal processing methods have been proposed for EEG feature extraction (Gudmundsson et al., 2007), but most of them have only focused on exploring specific channels that show extreme variation between conditions or groups. However, monitoring changes in the temporal configuration of rapidly fluctuating scalp potential maps is important and considered a practical and emerging approach for early detection of diseases (Milz et al., 2017). The scalp potential map tends to maintain a particular quasi-stable state, called a microstate (Lehmann et al., 1987), for a period of 60–120 ms; it then rapidly transitions to another microstate. EEG microstate analysis aims to explore large-scale neural networks by combining temporal and spatial EEG information and measuring the dynamics of the scalp potential topography (Michel and Koenig, 2017). A set of microstates, labelled as A to G (Custo et al., 2017), is generally considered to be the most representative topography, in which each microstate corresponds to specific neural networks in the resting state (Britz et al., 2010; Musso et al., 2010). Moreover, it is recognized that changes in cognitive and pathological states are usually associated with changes in microstate features (Michel and Koenig, 2017). For instance, an event-related potential study revealed that microstate topography relates to the performance of different tasks (Brandeis et al., 1995). This evidence motivated follow-up studies which found that different microstates dominate at different levels of consciousness (Brodbeck et al., 2012; Katayama et al., 2007). Furthermore, microstate features (e.g. topography, duration, coverage, and occurrence) have been found to be altered in schizophrenia (Kikuchi et al., 2007; Lehmann et al., 2005; Nishida et al., 2013), semantic dementia (Grieder et al., 2016), head injury (Corradini and Persinger, 2014), Alzheimer's disease (Nishida et al., 2013), stroke (Zappasodi et al., 2017), and panic disorders (Kikuchi et al., 2011). Due to this broad clinical evidence, microstates are a promising biomarker that may reveal the underlying relationships between EEG signals and brain function in various conditions.

Considering the above-mentioned evidence, it is necessary and worthwhile to study the reliability of microstate analysis and ensure the stability of outcomes with different experimental conditions. Many experimental conditions (including the amount of data, clustering algorithms, the number of clusters, smoothing parameters, and preprocessing strategies) have the potential to interfere with EEG microstate analysis and may cause negative effects. Of these experimental conditions, electrode configuration is one of the most important experimental conditions that needs to be seriously considered in microstate analysis, as different electrode densities may alter scalp potential topography dynamics at different resolutions. For instance, several studies of schizophrenia patients using different numbers of electrodes have concluded that the microstate with a central maximum polarity has a shorter duration than that of healthy control subjects (Kikuchi et al., 2007; Lehmann et al., 2005; Nishida et al., 2013). However, one of these studies using a 21-channel EEG revealed that the microstate with left posterior-right anterior polarity had a shorter duration (Nishida et al., 2013), while another two studies using 27-channel EEG (Lehmann et al., 2005) and 14-channel EEG (Strelets et al., 2003) did not observe the same phenomenon, suggesting that the number of channels may affect the consistency of the results. There are also several published studies on the consistency and reliability of microstates. For example, in one study, the inter-study and inter-individual consistency of microstate sequences were analysed through five different oral picture naming studies (Laganaro, 2017). The stability of five different microstate clustering algorithms was compared in terms of the following metrics: similarity, global explained variance, and entropy changes. There were no significant differences (von Wegner et al., 2018). Another study examined the test-retest reliability of different algorithms (specifically k-means clustering and topographic atomise agglomerate hierarchical clustering), different clustering approaches (global, session, and recording), and different numbers (30, 19, and 8) of channels. The results showed that the global clustering approach could obtain more stable microstates, and all three electrode configurations demonstrated high test-retest reliability (Khanna et al., 2014).

To the best of our knowledge, there are no reliable studies that present conclusive findings on the issue of the number of channels that provides reliable results, and related existing studies have only focused on microstate analysis in the resting state (Khanna et al., 2014). Thus, the current study aimed to investigate the reliability of EEG microstate features at different electrode densities during propofol-induced changes in brain states. The number of channels used in this study ranged from 8 to 91, covering the numbers of channels used in recent studies (Michel and Koenig, 2017). The methodology of the current study was divided into two parts. In the first part, the reliability of microstates was tested in the baseline and the moderate sedation conditions, respectively. For each condition, we examined whether similar microstate topographies could be obtained by clustering at five different electrode densities (91, 64, 32, 19, and 8 channels). Then, six types of microstate parameters (Duration, Coverage, Occurrence, GFP peaks per second, Transition Probability, and Entropy Rate) were compared at the five electrode densities. The intraclass correlation coefficient (ICC) and coefficient of variation (CV) were used to evaluate the consistency of the microstate parameters. In the second part, the reliability of microstate parameter features during propofol-induced changes in brain states was tested at five different electrode densities.

2. Methods

This study explored microstate reliability in the baseline condition and the moderate sedation condition, respectively. The consistency of features during transitions of consciousness at different electrode densities was also investigated. A diagram outlining the data analysis protocol is shown in Fig. 1.

2.1. Data recording and preprocessing

The experimental dataset was obtained from the open-access section of the University of Cambridge Data Repository (https://www.repository.cam.ac.uk/handle/1810/252736). The dataset contains well-processed EEG data from 20 healthy subjects (male/female=9/11; mean age=30.85, SD=10.98) during propofol injection. During the experiment, the brain states of the subjects were divided into four conditions: baseline (BS), mild sedation (ML), moderate sedation (MD), and the recovery stage (RC), where each condition lasted approximately 7 min. A computerised syringe driver (Alaris Asena PK, Carefusion, Berkshire, UK) was used to control the infusion of propofol and maintain the target concentration. A blood plasma level of 0.6 μg/ml corresponds to mild sedation and 1.2 μg/ml corresponds to moderate sedation. The electrical activity of the brain was collected using a 128-channel EEG amplifier at a 250 Hz sampling rate, referenced to the vertex. Each subject had their eyes closed during EEG data collection. All data preprocessing steps were implemented using the EEGLAB toolbox installed in Matlab. Channels on the neck, cheeks, and forehead were excluded because these channels are more susceptible to movement-related noise. Ultimately, 91 channels were retained for further EEG analysis. The raw data was filtered between 0.5 and 45 Hz and then segmented into 10-second epochs. Each epoch was baseline-corrected relative to the mean voltage of the epoch. A quasi-automated program was used to reject data that contained excessive eye movements or muscle artifact; this involved calculation of the normalised variance and manual choice of whether to retain it. After removing epochs with poor signal quality, each subject had at least 30 epochs in each section for subsequent EEG analysis (Chennu et al., 2016). By spatially down-sampling from 91 channels of EEG signals to 64, 32, 19, and 8 channels of EEG signals, 5 newly generated EEG datasets with different electrode densities were obtained for microstate analysis. The 5 electrode distributions were configured according to

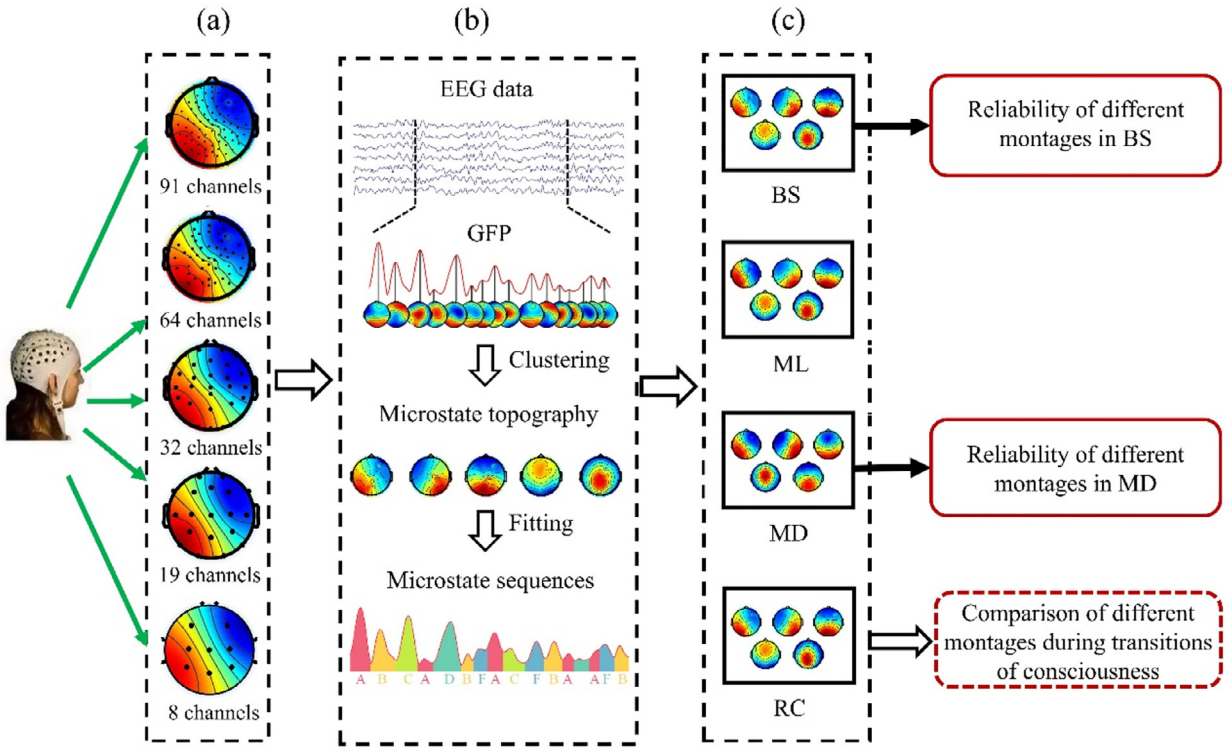

Fig. 1. The protocol for data analysis. (a) Topographic configurations with 5 different electrode densities. (b) Illustration of microstate clustering. The GFP curve of the multi-channel EEG was calculated to measure the strength of the scalp potential. The EEGs at the GFP local maximum points were selected for clustering purpose. The microstates obtained by clustering were fit back to the continuous EEG data to obtain the microstate sequences. (c) The whole propofol-induced transition procedure was divided into four conditions: baseline (BS), mild sedation (ML), moderate sedation (MD), and the recovery stage (RC). Please note that the number of clusters in the figure is assumed to be 5, and the optimal number of clusters varied depending on the dataset and method.

the modified 10-20 system, as illustrated in Fig. 1 (a).

2.2. Microstate analysis

Microstate analysis consisted of three steps: clustering, fitting, and parameter calculation.

The clustering and fitting process is illustrated in Fig. 1 (b). The multi-dimensional data at each sampling point was analysed as an independent EEG map. Global Field Power (GFP) was used to quantify the strength of the scalp potential and is equal to the standard deviation of all channel potentials at each sampling point. The local maximum position of GFP is considered to have the optimal signal-to-noise ratio and stable topography. Therefore, the maps corresponding to the local maximum of GFP were selected to conduct further microstate clustering and fitting (Skrandies, 1990). All selected maps were clustered using the modified k-means algorithm, which is a mature clustering method widely used in many microstate studies (Michel and Koenig, 2017). The number of clusters was determined by the Krzanowski-Lai (KL) criterion (Murray et al., 2008). Compared with the cross-validation method (Lai, 1988), the KL method is not sensitive to the number of electrodes; thus, it was deemed suitable for this study. The optimal number of clusters for each condition was based on the KL result of the 91-channel data that was calculated in an existing study (Shi et al., 2020).

A feature of the modified k-means algorithm is that the initial template is randomly selected, so the results of repeated calculations may be inconsistent. Global explained variance (GEV) is a measure of the degree to which the microstate clustering describes the dataset, and its value ranges between 0 and 1: the higher the value, the better the quality of the microstate analysis (Murray et al., 2008). Therefore, the GEV was compared to evaluate the quality of the results after clustering. Each clustering process was repeated 100 times, and the maps corresponding to the highest GEV were identified as the final microstates. Additionally, the polarity of maps was disregarded in the clustering computation.

Then, the continuous EEG was labelled according to the microstates. For each GFP peak, the spatial correlation between the EEG data and each microstate was calculated, and each sampling point was labelled as the microstate label with the highest correlation. For the data between GFP peaks, each point was labelled according to the label of the closet GFP peak. To keep the microstate label stable for a certain amount of time until it changed, a method of temporal smoothing was employed to eliminate rapid changes in microstate caused by noise in the microstate sequence (Pascual-Marqui et al., 1995). However, considering the compromise between goodness of fit and smoothness, the smoothing parameters were set as the window size parameter, b=1, and the non-smoothness penalty parameter, λ=0.05. These control parameters ensured that small segments of microstate with a temporal duration of less than 12 ms were rejected (Denis et al., 2011; Laganaro, 2017; Wang et al., 2021).

To more comprehensively measure the consistency of microstates at different electrode densities, the basic parameters and sequence-related parameters were calculated separately. The basic parameters included the parameters that are commonly calculated in microstate studies, including GFP peaks per second, Duration, Coverage, and Occurrence. *GFP peaks per second* is the average number of GFP peaks per second. *Duration* denotes the average duration of each occurrence of a current microstate before switching to another microstate. *Coverage* is the time coverage for each microstate in the whole time series. *Occurrence* represents the average number of occurrences per second for each microstate. It is worth mentioning that because of the discontinuity of epoch segmentation, the duration of the first and last microstates in each epoch was unknown; thus, these positions were not included in the calculation of Duration, Coverage, and Occurrence. The average value of each epoch parameter

for each subject was used as the final parameter for analysis. Sequence-related parameters are parameters that reflect the characteristics of a sequence, including Transition Probability and Entropy Rate. *Transition Probability* reflects the probability of each microstate transforming into another microstate. Transition Probability from A to B is the number of transitions from A to B divided by the number of all transitions from A to other microstates. *Entropy Rate* is a measure of the temporal property of a microstate sequence; it quantifies how much uncertainty is produced by increasing the length of the observed "characteristic sequence" (von Wegner et al., 2017). The complexity of the EEG sequence changes as the brain state changes (Wang et al., 2019). Based on the definition of Shannon entropy, joint entropy is designed to quantify the entropy value under different microstate sequence lengths. Joint entropy was calculated as follows,

$$h_n = -\sum_{x_1,\ldots,x_n} p(x_1,\ldots,x_n)\log\, p(x_1,\ldots,x_n) \tag{1}$$

where h_n represents joint entropy when the characteristic sequence length is n, $x_1,\ldots,x_n$ represents a continuous microstate sequence, and $p(x_1,\ldots,x_n)$ represents the probability of this particular microstate sequence appearing in the entire sequence. The joint entropy value changes as the length n of the characteristic sequence changes. The Entropy Rate is calculated as the slope of the linear least-squares fit of n and h_n. Due to the limited length of each epoch, accurate joint entropy estimation could not be obtained when n was large. Here, the entropy of the characteristic sequence length from 1 to 6 was selected to estimate the Entropy Rate.

2.3. Reliability analysis of EEG microstates

2.3.1. Reliability at different electrode densities in the BS condition

In the BS condition, 5 datasets with different electrode densities were analyzed as described above; the number of clusters was set to 4. Five sets of microstate maps and parameters were obtained and compared. First, the microstate label at 91-channel resolution was visually defined based on the distinct topological patterns reported in previous studies (Custo et al., 2017). The labels at other electrode densities were determined based on Pearson correlation coefficients (PCCs). Specifically, PCCs were computed between each microstate map in the 91-electrode configuration and those in the 64-, 32-, 19-, and 8-electrode configurations. Since the vector sizes of the microstates at different electrode densities are different, only the channels shared between two groups were selected for PCC calculation. The higher the PCC, the better the spatial correlation between the two microstates. Therefore, the labels for each map were determined based on the microstate with the highest PCC at the 91-channel resolution. Second, analysis of variance (ANOVA) was performed to check whether the electrode density influenced each microstate parameter. For the parameters with significant differences, post-hoc paired *t-tests* with Bonferroni correction for multiple comparisons were conducted to determine which two groups were significantly different. Finally, the ICC and CV were introduced to quantify the consistency of microstate parameters between the 5 different electrode densities. The ICC is a common indicator to evaluate test re-test and inter-observer reliability (Ip et al., 2018). The ICC increases as the intra-class variance reduces and the inter-class variance increases. Considering the characteristics of the data, a two-way random model was selected to calculate the average absolute agreement (Shrout and Fleiss, 1979). For this, the parameter values for each subject at all 5 electrode densities were within class, while the parameter values of different subjects were between classes. The smaller the parameter difference under the different electrode densities for the same subject and the greater the parameter difference between subjects, the higher the ICC. Paired *t-tests* were used to examine whether there were ICC differences between the various EEG electrode density combinations. The ICC calculation formula for the two-way random model was as follows,

$$ICC = \frac{MS_R - MS_E}{MS_R + (MS_c - MS_E)/n} \tag{2}$$

where MS_R represents the mean square for rows, MS_C represents the mean square for columns, and MS_E represents the mean square error. The CV is a measure of dispersion and is defined as the standard deviation divided by the mean (Shoukri et al., 2008). In this part, the dispersion of each parameter in the 5 electrode configurations was quantified. When neither the subjects nor the observations were unique, the mean and standard deviation were calculated as follows,

$$\mu = \frac{1}{n*k}\sum_{i=1}^{n}\sum_{j=1}^{k} y_{ij} \tag{3}$$

$$\sigma = \sqrt{\frac{1}{n*k}\sum_{i=1}^{n}\sum_{j=1}^{k}\left(y_{ij} - \frac{1}{k}\sum_{j=1} y_{ij}\right)^2} \tag{4}$$

where y_{ij} denotes the parameter of the ith subject under the jth configuration, n represents the number of subjects, and k represents the number of configurations.

2.3.2. Reliability among different electrode densities in the MD condition

Microstate analysis was performed on 5 datasets in the MD condition; the number of clusters was set as 5 (Shi et al., 2020). The PCCs between the maps in the 91-channel configuration and the corresponding maps in the other configurations were calculated to test if the microstate maps were stable at different electrode densities. Each microstate parameter was subjected to the same statistical analysis and consistency analysis as described in Section 2.3.1.

2.3.3. Comparison of the different electrode densities during propofol-induced transitions of consciousness

To investigate whether the same inter-state microstate characteristics were observed at the different electrode densities, the EEG microstates in the 4 brain-state conditions were reanalysed with the cluster number set to 5. In our previous study, a microstate analysis of 91-channel EEG revealed significant differences in some parameters between the BS and MD conditions (Li et al., 2020; Shi et al., 2020). Therefore, this study evaluated whether these differences varied with electrode density. In this study, the coverage of microstate C (Coverage C), the coverage of microstate F (Coverage F), the duration of microstate C (Duration C), and the occurrence of microstate F (Occurrence F) were compared across the different electrode densities and paired *t-tests* were used to check whether the significant differences remained stable. Moreover, statistical analysis (paired *t-tests* or Wilcoxon signed-rank tests, determined by the characteristics of the data) was conducted on the Transition Probability and Entropy Rate in the BS and MD states to explore whether the transition trend and complexity of the microstate sequence changed with changes in the brain state. Finally, all parameters that were significantly different between the BS and MD conditions were used as feature inputs to a support vector machine (SVM) classifier in order to distinguish EEG in the MD condition from EEG in the BS condition. The RBF kernel was selected, and the best parameters C and $gamma$ were selected by grid optimization (Cortes and Vapnik, 1995). The leave-one-out-cross-validation (LOOCV) strategy was chosen to evaluate the classification results. As each case was tested once, the results were combined to generate a receiver operating characteristic (ROC) curve. Then, the area under the curve (AUC) was calculated to quantify the classification performance.

In addition, the consistency of the state parameters during changes of consciousness were measured by ICCs. Here, the changes in brain states (BS, ML, MD, and RC) for each subject were analysed separately. The parameter values for the same condition at the 5 electrode densities were within the same class. The parameter values for the different conditions were between classes. The smaller the parameter difference between the

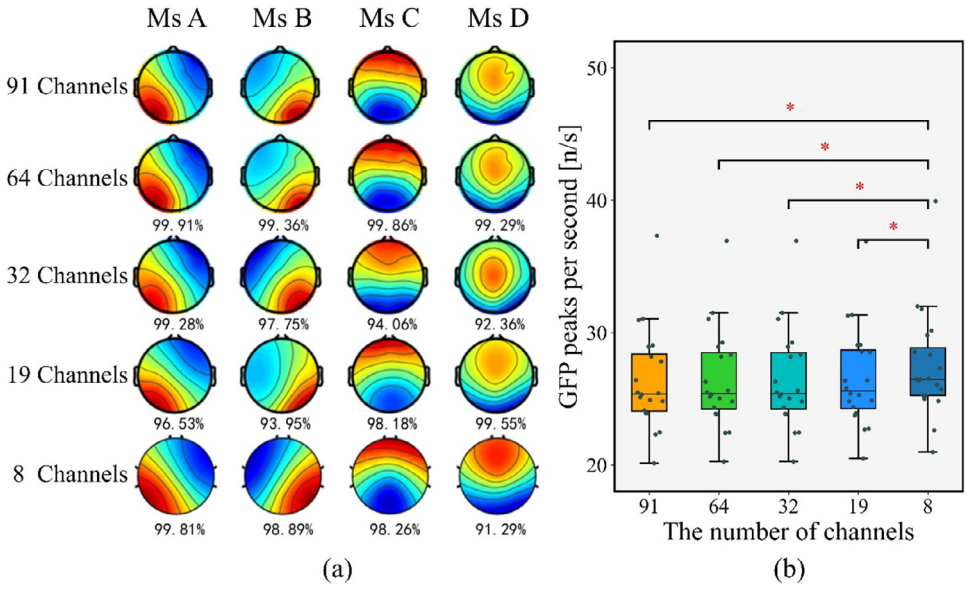

Fig. 2. (a) Topographies of the BS microstates at the 5 electrode densities. The maps are labelled as microstate A, B, C, and D. Pearson correlation coefficients between microstates at 64-, 32-, 19-, or 8-channel resolution and the corresponding microstate at 91-channel resolution are marked under the topographies. (b) Boxplots of GFP peaks per second in the BS condition under different electrode densities. The bar of each subgraph is the standard deviation. Ms: Microstate. *:$p<0.005$ (Bonferroni corrected).

different electrode densities in the same condition and the greater the parameter difference between the different conditions, the higher the ICC.

3. Results

3.1. Reliability in the BS condition

Five sets of microstate maps at different electrode densities under the BS condition are shown in Fig. 2 (a). The PCCs between the microstates at the 91-channel resolution and the microstates at other configurations ranged from 0.91 to 0.99. Each set of microstate maps matched the generally accepted microstates A, B, C, and D. GFP peaks per second at different configurations is compared in Fig. 2 (b). The average GFP peaks per second ranged between 26.38 and 27.46. There were significant differences between the parameters from the 8-channel configuration and the parameters at the other 4 configurations.

The results for the Duration, Coverage, and Occurrence parameters at the different electrode densities are illustrated in Fig. 3. Comparison of the data in the left 4 columns suggests that these parameters were not as highly consistent as GFP peaks per second. For the 5 datasets with different electrode densities, the microstate analysis results were not consistent. The right-most column shows the statistical analysis results. A line between two nodes indicates that there was a significant difference between the related two electrode densities; the line colour indicates the corresponding microstate. For Duration and Coverage, there were no significant differences between the 91-, 64-, and 32-channel configurations. All the differences occurred between the 19-channel or 8-channel configurations and the other configurations. For Occurrence, apart from the differences between the 32-channel configuration and both the 91-channel and 64-channel configurations in microstate D, the other differences were all between the 19-channel or 8-channel configuration and the other configurations.

Table 1 provides a descriptive summary of the ICC and CV data in the BS condition. The consistencies of the 91 vs. 64 vs. 32 vs. 19 vs. 8 (5 kinds of electrode densities, 5KED), 91 vs. 64 vs. 32 vs. 19 (4 kinds of electrode densities, 4KED), and 91 vs. 64. vs. 32 (3 kinds of electrode densities, 3KED) in the BS condition were calculated separately. The average ICC and CV of 5KED were 0.91 (SD=0.08) and 13.74% (SD=9.13%), respectively. The average ICC and CV of 4KED were 0.92 (SD=0.07) and 12.42% (SD=9.13%), respectively. The average ICC and CV of 3KED were 0.95 (SD=0.04) and 9.79% (SD=7.48%), respectively.

Table 1
Descriptive summary of the ICCs and CVs of the basic parameters in the BS condition.

Parameter	Ms	91vs64vs32vs19vs8		91vs64vs32vs19		91vs64vs32	
		ICC	CV	ICC	CV	ICC	CV
Duration	A	0.96	6.02%	0.96	5.38%	0.98	3.54%
	B	0.97	4.70%	0.96	4.57%	0.97	3.69%
	C	0.94	10.37%	0.95	8.80%	0.97	6.22%
	D	0.94	12.92%	0.94	12.52%	0.96	9.16%
Coverage	A	0.92	12.99%	0.95	10.93%	0.96	9.19%
	B	0.89	11.92%	0.9	10.63%	0.93	7.56%
	C	0.69	16.93%	0.74	14.78%	0.85	10.86%
	D	0.87	32.96%	0.9	31.85%	0.94	25.65%
Occurrence	A	0.98	8.04%	0.99	6.17%	0.99	5.88%
	B	0.97	9.35%	0.98	7.42%	0.98	5.81%
	C	0.94	7.85%	0.95	6.80%	0.96	5.37%
	D	0.8	30.89%	0.86	29.23%	0.91	24.53%
STD		0.08	9.13%	0.07	9.00%	0.04	7.48%
Average		0.91	13.74%	0.92	12.42%	0.95	9.79%

The statistical analysis showed that the ICCs of each paired comparison of 5KED, 4KED, and 3KED were significantly different. The ICC of 3KED was higher than that of 4KED and 5KED, while the opposite trend was seen for the CV.

Changes in the transition probability of each pair of microstates and the results of the statistical analysis are shown in Supplementary Fig. S1. For all 16 different microstate transitions, the difference in parameters mainly existed between the 19-channel or 8-channel configuration and the other configurations. The ICC and CV of Transition Probability in the BS condition are shown in Table S1. Based on 3KED, adding 19- and 8-channel configurations in sequence gradually reduced the average ICC and increased the CV. The results for the Entropy Rate in the BS condition at different electrode densities are shown in Fig. S2. Entropy Rate in the BS condition exhibited the same trends as GFP peaks per second. When the number of channels was no less than 19, the Entropy Rate remained stable; when there were 8 channels, the Entropy Rate was significantly different from the results of the other 4 configurations.

3.2. Reliability in the MD condition

Five sets of microstate maps under the MD condition are shown in Fig. 4(a). The PCCs of microstates D and F were less than 0.9 in the 19-

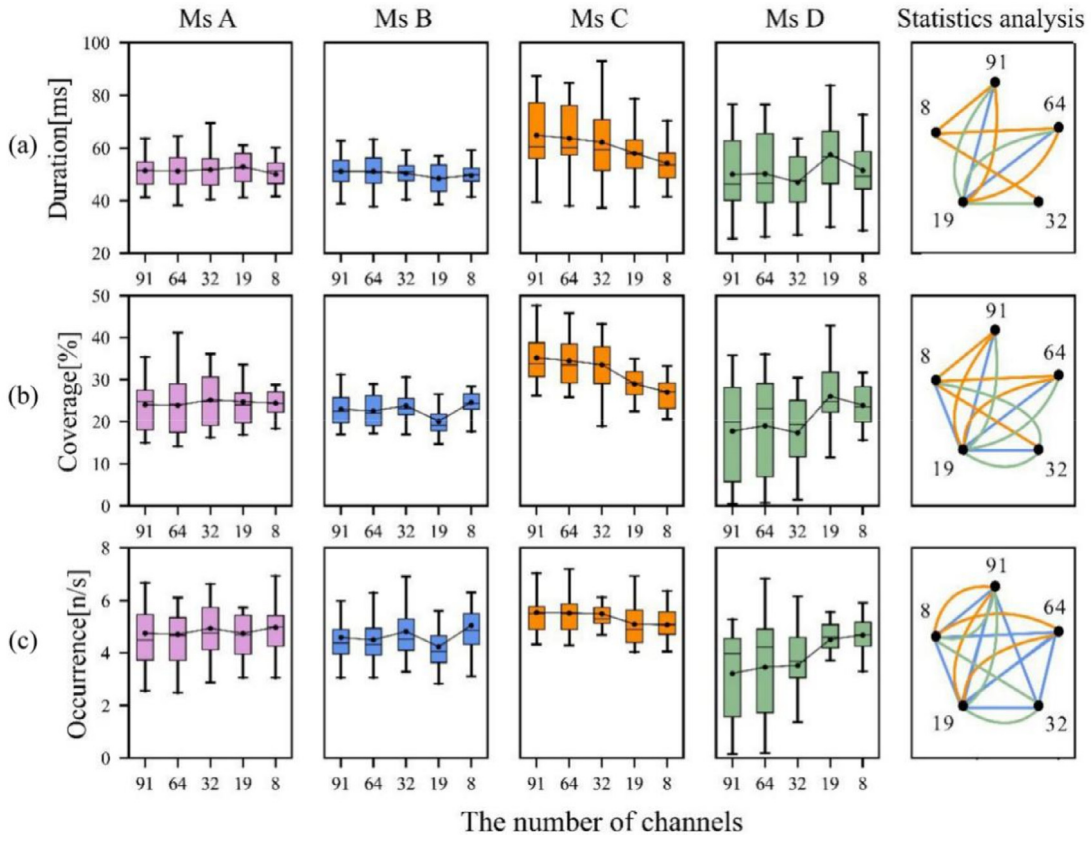

Fig. 3. Group comparison of (a) Duration, (b) Coverage, and (c) Occurrence in the BS condition at different electrode densities. The 4 columns on the left are descriptive graphs of the microstate parameters. The right-most column is the result of statistical analysis. A line between two nodes indicates that these two configurations are significantly different, and the colour of the line marks the corresponding microstate. The bar in each subgraph is the standard deviation. All statistical differences are Bonferroni corrected. Ms: Microstate.

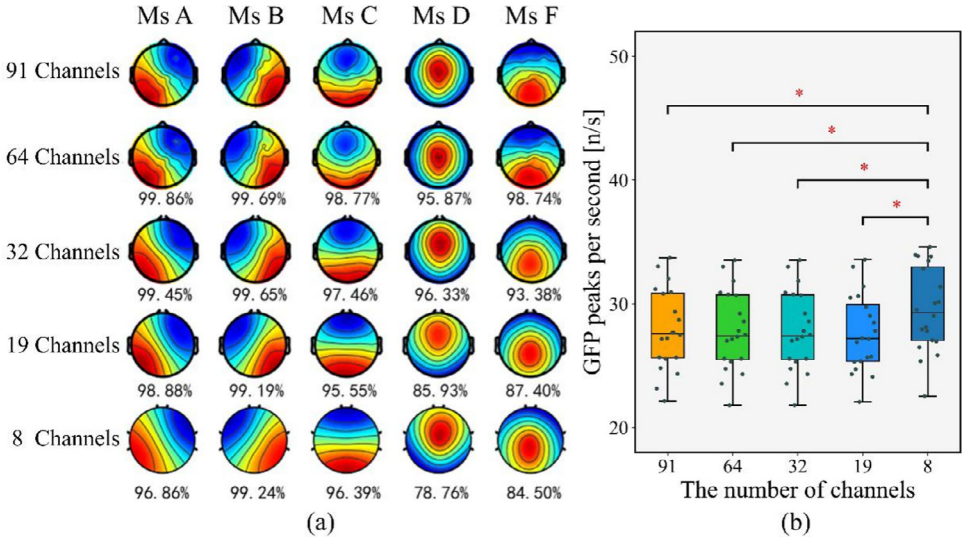

Fig. 4. (a) Topographies of MD microstates at 5 electrode densities. The maps are labelled as microstates A, B, C, D, and F. The PCCs between the microstates at 64-, 32-, 19-, or 8-channel resolution and the corresponding microstate at 91-channel resolution are marked under the topographies. (b) Boxplots of GFP peaks per second in the MD condition at different electrode densities. The bar in each subgraph is the standard deviation. Ms: Microstate. *:$p<0.005$ (Bonferroni corrected).

channel configuration and the PCC of microstate D was less than 0.8 in the 8-channel configuration. Fig. 4(b) reports the results of GFP peaks per second in the MD condition. Compared with the BS condition, the GFP peaks per second value fluctuated more markedly in the MD condition (range from 27.63 to 29.53). The statistical analysis showed that GFP peaks per second at the 8-electrode configuration was significantly different from the GFP peaks per second values in the other 4 configurations.

The descriptive statistics and ANOVA results for the Duration, Coverage, and Occurrence parameters are shown in Fig. 5. Except for the differences between the 32-channel, 64-channel, and 91-channel configurations in microstate F, the other differences were all between the 19-channel or 8-channel configurations and the other configurations.

Table 2 provides a descriptive summary of the ICC and CV data in the MD condition. The average ICC and CV of 5KED were 0.87 (SD=0.10) and 16.33% (SD=8.51%), respectively. The average ICC and CV of 4KED

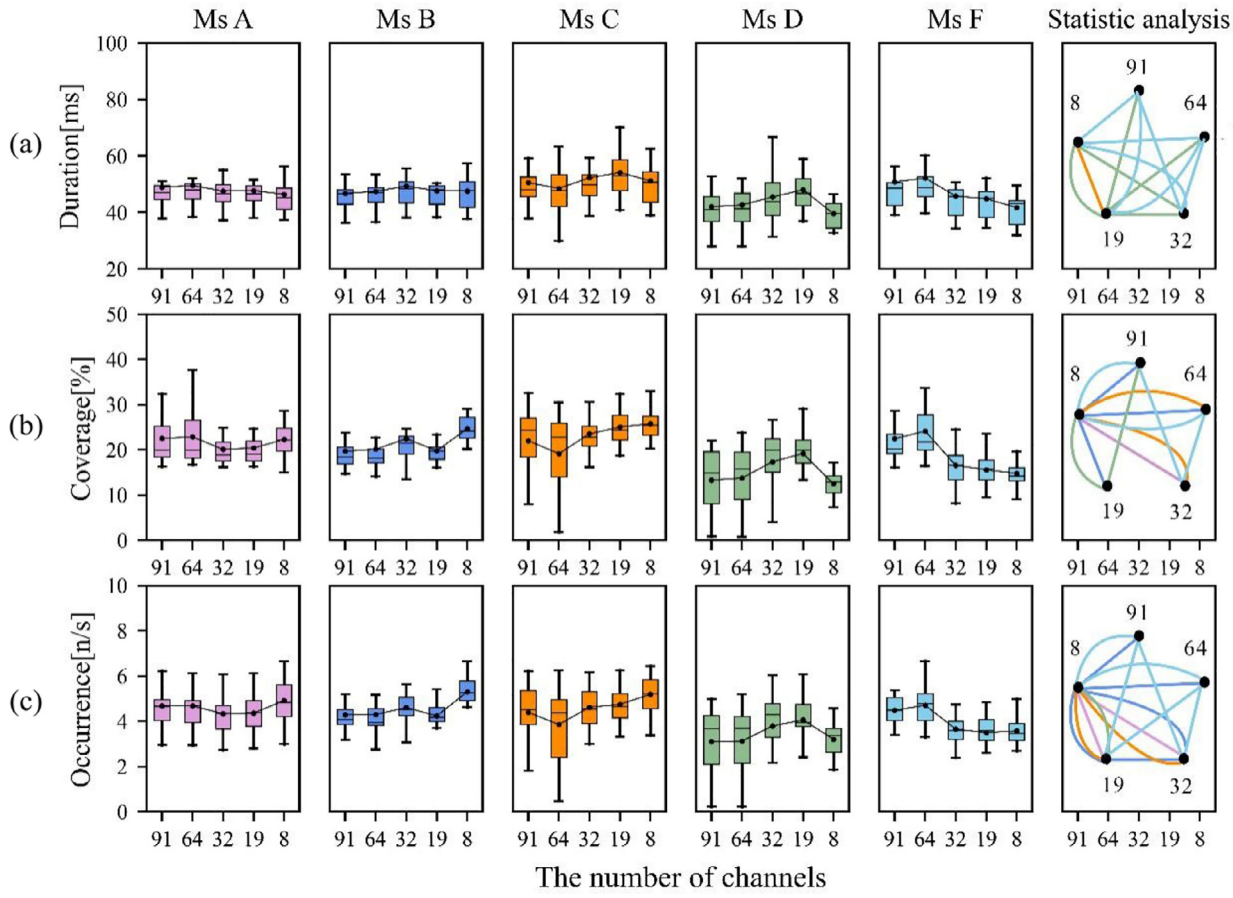

Fig. 5. Group comparison of (a) Duration, (b) Coverage, and (c) Occurrence in the MD condition at different channel numbers. The 5 columns on the left are the mean-standard deviation graphs of the microstate parameters. The right-most column is the result of statistical analysis. A line between two nodes indicates that these two configurations are significantly different, and the colour of the line denotes the corresponding microstate. The bar in each subgraph is the standard deviation. All statistical differences are Bonferroni corrected. Ms: Microstate.

Table 2
Descriptive summary of ICC and CV results in the MD condition.

Parameter	ms	91vs64vs32vs19vs8		91vs64vs32vs19		91vs64vs32	
		ICC	CV	ICC	CV	ICC	CV
Duration	A	0.96	7.03%	0.96	6.27%	0.96	5.49%
	B	0.99	4.43%	0.99	4.13%	0.98	4.48%
	C	0.96	8.83%	0.94	9.15%	0.94	8.28%
	D	0.92	10.53%	0.92	9.86%	0.92	9.00%
	F	0.94	11.98%	0.95	10.23%	0.95	9.11%
Coverage	A	0.85	15.27%	0.85	15.17%	0.86	14.16%
	B	0.89	14.70%	0.94	11.33%	0.94	10.96%
	C	0.74	22.26%	0.74	23.29%	0.77	23.65%
	D	0.83	32.22%	0.84	30.53%	0.87	28.96%
	F	0.65	30.01%	0.64	28.83%	0.65	25.58%
Occurrence	A	0.95	9.29%	0.96	8.10%	0.95	7.72%
	B	0.9	12.39%	0.96	7.42%	0.96	6.84%
	C	0.84	19.37%	0.83	19.63%	0.85	21.10%
	D	0.88	26.92%	0.88	26.57%	0.9	24.74%
	F	0.69	19.71%	0.68	20.21%	0.68	18.30%
STD		0.1	8.51%	0.11	8.77%	0.1	8.35%
Average		0.87	16.33%	0.87	15.38%	0.88	14.56%

were 0.87 (SD=0.11) and 15.38% (SD=8.77%), respectively. The average ICC and CV of 3KED were 0.88 (SD=0.10) and 14.56% (SD=8.35%), respectively. Statistical analysis showed that the ICC of 3KED was significantly different from that of 4KED and 5KED. Combining the numerical and statistical analysis results, the consistency was high between the 91-, 64-, and 32-channel configurations, and when the 19- and 8-channel configurations were introduced, the consistency decreased.

The Transition Probability results in the MD condition are shown in Fig. S3. For all 25 different microstate transitions in the MD condition, the results from the 91- and 64-channel configurations were stable. As the electrode density decreased, the stability of the parameter results decreased, and the magnitude of the significant differences between the results at different electrode densities increased. The ICC and CV of Transition Probability in the MD condition are shown in Table S2. The results for the ICC and CV of Transition Probability compared to the basic parameters are poor; the ICC was lower and CV was higher at the same electrode density combinations. However, the consistency of 3KED was still higher than that of 5KED. The results for the Entropy Rate in the MD condition are shown in Fig. S4. The Entropy Rate remained stable when more than 19 channels were used; a significant change was observed at 8-channel resolution, which is consistent with the result in the BS condition.

3.3. Comparison during propofol-induced transitions of consciousness

Fig. 6 depicts the comparison of the 4 basic parameters in the BS and MD conditions. For the 91-electrode configuration, there were significant differences between the two conditions (BS and MD) for all 4 parameters. These results are as expected. In the 64-and 32-electrode configurations, most of the differences observed between the BS and MD conditions remained stable. However, in the 19- and 8-electrode configurations, the significant differences observed at higher electrode

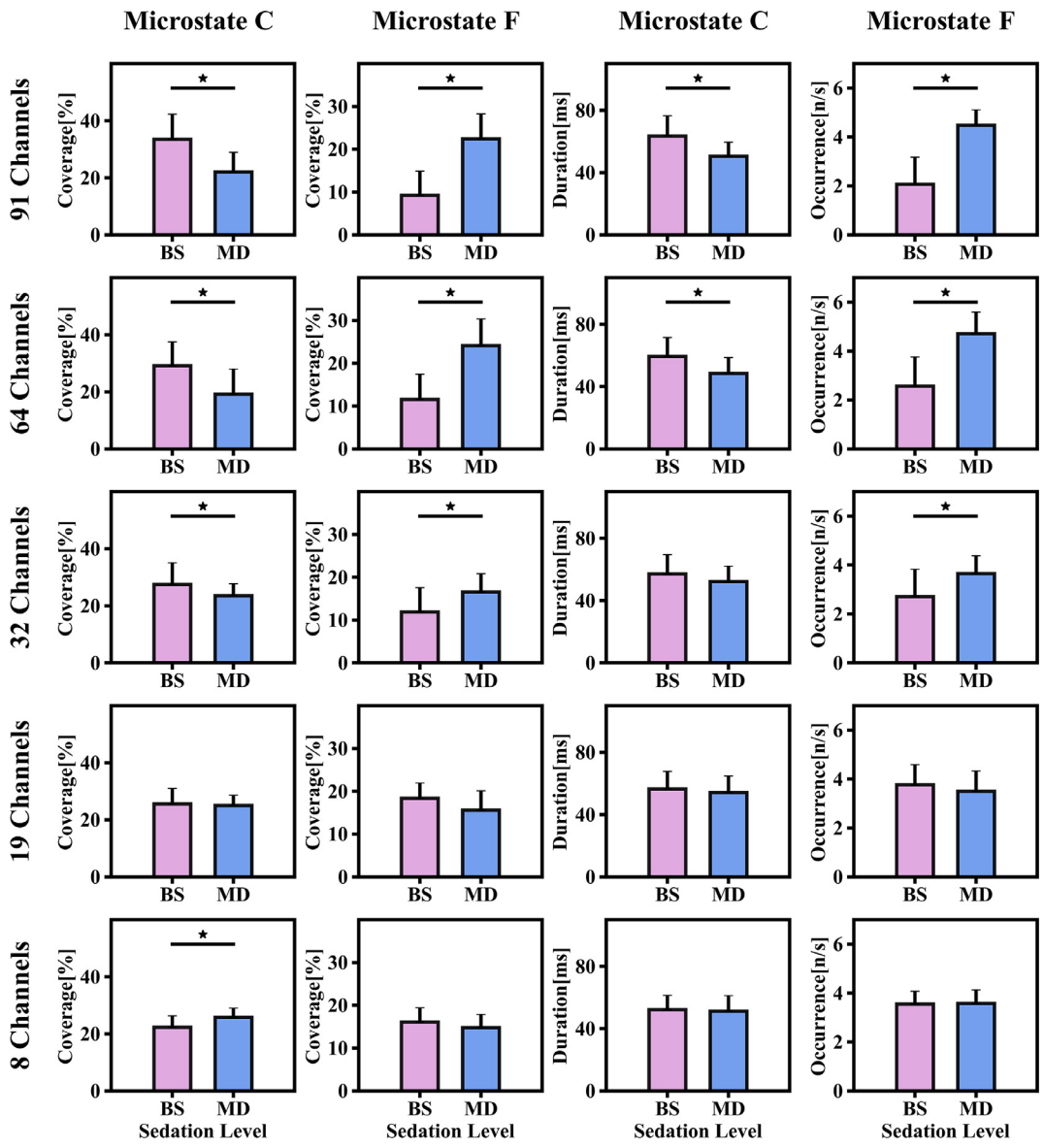

Fig. 6. Comparison of Coverage C, Coverage F, Duration C, and Occurrence F between the BS and MD conditions during change of consciousness measured using different electrode densities. The bar in each subgraph is the standard deviation. Significant differences are marked in the figures. All statistical differences have been Bonferroni corrected

densities were no longer present. In addition, Coverage C showed opposing significant differences in the 8-channel configuration.

The comparison of sequence-related parameters in the BS and MD conditions is shown in Fig. S5. The transition probabilities of microstates A to C, B to C, D to C, and F to C for the 91-channel configuration were significantly different between the BS and MD conditions. Repeated comparisons revealed that some of the differences were absent in the 19- and 8-channel resolutions.

The 8 parameters that were significantly different between the BS and MD conditions were input as features in the SVM classification for the 91-, 64-, 32-, and 19-channel configurations. However, only 7 parameters were input for the 8-channel data because Coverage C exhibited opposite effects at the 8-channel resolution. The ROC curves of the parameters obtained by the SVM classifier are shown in Fig. 7. The AUCs of classification for the 91-, 64-, 32-, 19-, and 8-electrode configurations were 0.950, 0.940, 0.875, 0.660, and 0.748, and the classification accuracies were 97.5%, 92.5%, 80%, 65%, and 62.5% respectively. These results demonstrate that differentiation between the BS and MD conditions decreased as the electrode density decreased.

The mean inter-state consistency results at the subject-group level are shown in Table 3. The average ICCs of 10 parameters in 5KED and 9 parameters in 4KED were lower than 0.8. Only 6 ICCs of 3KED were below 0.8. When the electrode density was insufficient, there were large intra-group differences and small inter-group differences between the different levels of consciousness for each of the parameters.

4. Discussion

Spatial analysis of EEG using microstates has been widely utilised to reveal the specific neural mechanisms in the process of brain state changes. However, it remains unknown whether the electrode density used to measure EEG will affect the reliability of microstate analysis. For example, our previous high-density EEG research showed that, associated with the default mode network, microstate C exhibited some changes during transitions of consciousness (Shi et al., 2020); however, it was not clear whether lower-density EEGs could detect this change. In the current study, the reliability of microstates at different electrode densities was tested during propofol-induced transitions of conscious-

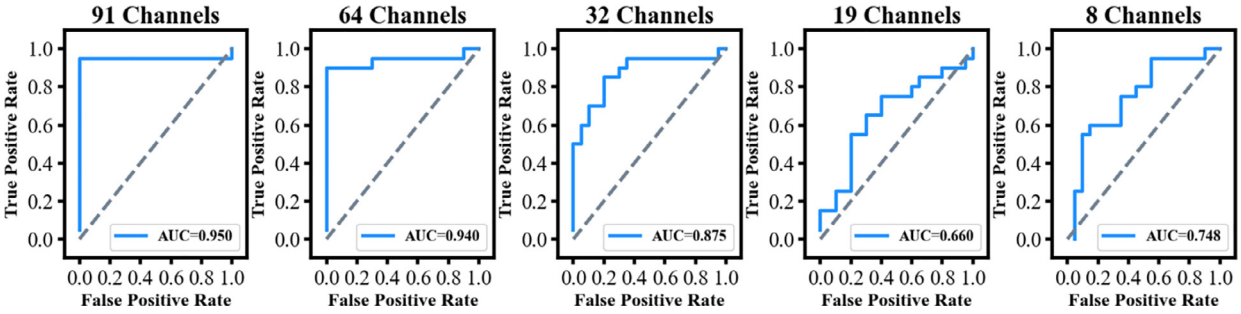

Fig. 7. ROC curve of SVM classification between the BS and MD conditions is shown in the right-most column. The area under curve (AUC) was calculated and is marked in the graphs. BS: baseline, MD: moderate sedation, ROC: receiver operating characteristic, AUC: area under curve.

Table 3
Descriptive statistics summary of ICC during propofol-induced transitions.

Parameter	ms	91vs64vs32vs19vs8		91vs64vs32vs19		91vs64vs32	
		mean	std	mean	std	mean	std
Duration	A	0.9	0.15	0.94	0.05	0.95	0.04
	B	0.94	0.06	0.96	0.03	0.95	0.04
	C	0.8	0.25	0.83	0.24	0.85	0.22
	D	0.8	0.16	0.82	0.24	0.86	0.2
	F	***0.78***	0.26	***0.78***	0.23	0.84	0.21
Coverage	A	***0.66***	0.32	***0.72***	0.35	***0.74***	0.35
	B	***0.59***	0.31	***0.74***	0.21	***0.73***	0.25
	C	***0.66***	0.25	***0.69***	0.27	***0.73***	0.22
	D	***0.67***	0.26	***0.72***	0.31	0.8	0.25
	F	***0.55***	0.34	***0.67***	0.28	0.81	0.17
Occurrence	A	0.82	0.22	0.89	0.11	0.88	0.13
	B	***0.74***	0.28	0.81	0.27	0.8	0.3
	C	***0.73***	0.24	***0.79***	0.22	***0.77***	0.23
	D	***0.66***	0.34	***0.69***	0.37	***0.74***	0.34
	F	***0.59***	0.31	***0.68***	0.3	***0.79***	0.22

ness. It was expected that the minimum recommended number of electrodes would be determined for use in future microstate analysis. Based on the previously analysed 91-channel dataset, 5 datasets with different electrode densities were analysed by manually removing some channels from each dataset. The following text will discuss the stability of microstate topography, the microstate parameters in each condition, and the microstate features between different conditions at different electrode densities.

The correlations between microstate topographies at different electrode densities were different between the BS and MD conditions. In the BS condition, using the 91-channel microstates as a template, all microstates under the 64-, 32-, 19-, and 8-channel configurations had excellent PCC values. Microstates A, B, C, and D are a group of typical microstates that are stable in the resting state and can generally be recognised in most studies using different electrode densities (Khanna et al., 2015; Michel and Koenig, 2017). The topographic map of microstates A, B, C, and D explained more global variance than the other special microstates (Custo et al., 2017). However, in the MD condition, as the number of channels decreased, the PCC decreased to below 0.9, or even less than 0.8 in certain situations. We propose that the differences in clustering numbers may be a reason for this variation, as mentioned in some earlier studies (Lai, 1988; Murray et al., 2008). In the MD condition, since the clustering number was set to 5, in addition to the 4 stable microstates, any new microstate that occupied a small proportion of the time series would reduce the difference between the classes, which, in turn, would increase the likelihood that each sampling point would be clustered into different classes in the different electrode configurations (Pascual-Marqui et al., 1995). The results showed that microstates D and F were mostly affected. The larger the difference in the number of channels, the greater the possibility of a sampling point being classified into a different cluster under different electrode configurations. In particular, the maps of microstates D and F at 8-channel resolution varied greatly compared with that at 91-channel resolution. Further, there was an interesting phenomenon whereby microstate F in the 64-channel configuration looked more visually similar to class C than microstate C in the 64-channel configuration. However, the Pearson correlation coefficient results showed that 64-channel microstate C and 91-channel microstate C were the most strongly correlated (0.987), while the Pearson correlation coefficient between 64-channel microstate F and 91-channel microstate C was 0.843. Therefore, labelling decisions for each microstate also have an impact on the results, and it is necessary to have a relatively defined, normative standard. There was also a notable difference in 91-channel microstate D between the BS and MD conditions, which may originate from the number of clusters. When the data were processed with 5 clusters, microstates D and F had a high degree of similarity but could still be defined separately. When the number of clusters was reduced to 4, microstates D and F were combined into 1 cluster. Further, for the same dataset, when different numbers of channels were selected for clustering, the microstate maps became inconsistent. Then, for different datasets, it should be considered that clustering maps are unlikely to be exactly the same. Therefore, although microstates in different research results are labelled the same, some topographical differences can potentially affect the consistency of any conclusions (Gschwind et al., 2016; Seitzman et al., 2017). This may provide an explanation for the inconsistent conclusions reported to date in multiple studies on schizophrenia. Therefore, to ensure consistency in clinical applications, the number of channels that provides stable results should be selected for microstate analysis.

At present, most of the existing studies on microstates primarily focus on the comparison of derived parameters (Drissi et al., 2016; Tomescu et al., 2015). The number and position of GFP peaks in EEG data plays an important role in microstate analysis (Mishra et al., 2020). The process of clustering and microstate fitting is based on the data corresponding to the position of GFP peaks (Corradini and Persinger, 2014). Therefore, if the number and position of GFP peak points vary significantly at different electrode densities, the clustering maps and parameters will be greatly affected. In the BS and MD conditions, although the numerical distributions showed little change under the 5 different electrode configurations, statistical analysis revealed significant differences between the 8-channel configuration and all other configurations assessed in this study. Therefore, the dataset corresponding to the GFP peaks using the 8-channel configuration was partly inconsistent with the datasets for the other 4 configurations. As a consequence, different clustering maps may be drawn on a dataset with 8 channels compared to datasets with more channels.

Further, in the BS and MD conditions, the reliability of the Duration, Coverage, Occurrence, Transition Probability, and Entropy Rate data at the 5 different electrode densities was measured. The stability of the Entropy Rate value was high, and the results at no fewer than 19-channel resolution were very stable. The numerical distributions of Duration, Coverage, and Occurrence, however, were not as consistent as GFP peaks per second. Statistical analysis showed that there were

few significant differences between the parameters when determined using 91, 64, or 32 channels; most differences were observed between the 19- or 8-channel configurations and the other configurations. This result indicates that when less than 20 channels are used, the resulting parameters may have low stability and consistency. When the electrode density was low, different results were produced with different numbers of channels. ICC and CV values are commonly used to evaluate outcome reliability. Here, we used them to measure the consistency of microstate parameters calculated at different electrode densities. The ICC and CV results were calculated for each of the 5KED, 4KED, and 3KED subgroups for both the BS and MD conditions. The results showed that the consistency among the 91-, 64-, and 32-channel configurations was excellent, but the consistency successively decreased when 19 channels and 8 channels were introduced. The reliability of the Transition Probability measurements at different electrode densities was worse than the above basic parameters. In the MD condition, the partial Transition Probability in the 32-channel configuration data was inconsistent with the Transition Probability measurements at higher electrode densities. The decreased consistency of the parameters at lower electrode densities may be linked to inconsistency between the dynamic process of the brain states recorded at low channel numbers versus those recorded at higher channel numbers. In other words, the description of topographic maps using different electrode densities is different. For example, when the electrode density is low, an EEG electrode records a “characteristic signal” that can explain the current brain state. Due to the low electrode density and the long distance between the electrodes, the surrounding electrodes cannot detect this “characteristic signal”. If this electrode is removed, the energy at the corresponding position of the topographic map will be replaced by the smoothed average value of the surrounding electrodes, resulting in a loss of detailed information originating from that particular location, which reflects the current underlying brain activity. Then, the same sampling point may be assigned to a different cluster, which affects any subsequent parameter calculations. However, when the electrode density is high enough, the same position may be sampled by more than one electrode; thus, the addition or deletion of partial electrodes will not seriously affect the overall topographic map. Therefore, a more realistic and consistent parameter result can be obtained by selecting a higher electrode density for microstate analysis. Moreover, compared to the A and B microstates, which have distinctive features in their spatial structures, the spatial structures of the C, D, and F microstates are relatively similar. This results in ICC and CV values for the C, D, and F microstates that are worse than those of microstates A and B.

Microstates, as an emerging biomarker, have been extensively used to compare features between consciousness-related conditions or participant groups (Comsa et al., 2019; Strik et al., 1995). This study revealed that microstate parameters change as electrode density changes. To evaluate if microstates can be a reasonable biomarker, we also tested the reliability of microstate features between different brain states. Eight parameters were shown to be significantly different between the BS and MD conditions. If these differences are stable and consistent, they should also be observed under other electrode configurations. The results showed that the microstate features of the 64- and 32-channel configurations exhibited the same significant differences as those observed at 91-channel resolution; however, some of the differences disappeared when the number of channels decreased to 19 or 8. The application of microstate features in classifications has wide-ranging prospects and it is of great significance to the diagnosis of diseases and the monitoring of brain states. If the same result cannot be generated using different electrode densities, it is impractical for use in clinical diagnosis. The classification results of the 4 microstate parameters showed that the fewer the number of channels, the worse the classification performance. The ICCs of the parameters between the 4 conditions also showed that the consistency of 91-, 64-, and 32-channel configurations was better. Therefore, the microstate features between different brain states remained stable and reliable at higher electrode densities. Based on the above results, the consistency and stability of microstate features between different brain states can be guaranteed when the number of channels used for EEG recording is no less than 32.

The current study has some limitations when assessing the reliability of brain microstates. First, the reliability of microstates was only assessed during moderate sedation and compared to baseline data in the same patients. Whether the reliability of other task states is consistent with that of sedation requires further investigation. Furthermore, only the electrode configuration was varied in the current study in order to identify whether it affected the consistency of the microstates. The influence of other experimental conditions, such as smoothing parameters and preprocessing strategies, also needs to be systematically explored using similarly vigorous methodologies so that any proposed guidelines can include recommendations for all the variables that may affect the reliability of microstate characterisation.

5. Conclusion

The present study analysed the influence of channel number on microstate analysis and provided the recommended number of channels for further microstate research. In this study, the reliability of microstates at different electrode densities was investigated. First, the reliability of microstate topography and parameters were measured in both a baseline and moderate sedation condition. Second, the reliability of any differences between microstate features during propofol-induced transitions of brain states was measured. The results showed that microstate analysis at 91-, 64-, and 32-channel resolution was more reliable and consistent. The conclusions obtained using low electrode density configurations were not as reproducible as those obtained with higher electrode densities. When conducting microstate analysis, it is recommended to use no less than 32-channel EEG data, and the channels should be evenly distributed on the scalp.

Data and code availability and statement

The EEG recordings were published and open-access in University of Cambridge Data Repository (https://www.repository.cam.ac.uk/handle/1810/252736), comprising of pretreated spontaneous EEG and behavioral data from 20 healthy participants (9 male, 11 female; mean age = 30.85; S.D = 10.98) during propofol-induced transition of consciousness with ethical approval provided by the Cambridgeshire 2 Regional Ethics Committee. All clinical investigations were conducted in line with the Declaration of Helsinki.

All the source codes and scripts with annotations are available upon request by contact with the corresponding author.

Declaration of Competing Interest

The authors declare no competing financial interests.

Credit authorship contribution statement

Kexu Zhang: Conceptualization, Methodology, Software, Formal analysis, Investigation, Writing - original draft, Writing - review & editing, Visualization. **Wen Shi:** Methodology, Software, Validation, Formal analysis, Investigation, Writing - review & editing. **Chang Wang:** Software, Formal analysis, Investigation, Writing - review & editing. **Yamin Li:** Software, Formal analysis, Writing - review & editing. **Zhian Liu:** Software, Formal analysis, Writing - review & editing. **Tun Liu:** Formal analysis, Data curation, Writing - review & editing. **Jing Li:** Formal analysis, Data curation, Writing - review & editing. **Xiangguo Yan:** Resources, Writing - review & editing, Project administration. **Qiang Wang:** Data curation, Writing - review & editing. **Zehong Cao:** Formal analysis, Writing - review & editing. **Gang Wang:** Conceptualization, Methodology, Formal analysis, Validation, Writing - review & editing, Visualization, Supervision, Project administration, Funding acquisition.

Acknowledgments

This work was supported in part by the National Natural Science Foundation of China under Grants 32071372, 31571000 and 61471291; in part by the Natural Science Basic Research Program of Shaanxi under Program No. 2020JM-037; and in part by the Fundamental Research Funds for the Central Universities of China under Grant xjj2017122.

Supplementary materials

Supplementary material associated with this article can be found, in the online version, at doi:10.1016/j.neuroimage.2021.117861.

References

Brandeis, D., Lehmann, D., Michel, C.M., Mingrone, W., 1995. Mapping event-related brain potential microstates to sentence endings. Brain Topogr. 8, 145–159.
Britz, J., Van De Ville, D., Michel, C.M., 2010. BOLD correlates of EEG topography reveal rapid resting-state network dynamics. Neuroimage 52, 1162–1170.
Brodbeck, V., Kuhn, A., von Wegner, F., Morzelewski, A., Tagliazucchi, E., Borisov, S., Michel, C.M., Laufs, H., 2012. EEG microstates of wakefulness and NREM sleep. Neuroimage 62, 2129–2139.
Chennu, S., O'Connor, S., Adapa, R., Menon, D.K., Bekinschtein, T.A., 2016. Brain connectivity dissociates responsiveness from drug exposure during propofol-induced transitions of consciousness. PLoS Comput. Biol. 12, e1004669.
Comsa, I.M., Bekinschtein, T.A., Chennu, S., 2019. Transient topographical dynamics of the electroencephalogram predict brain connectivity and behavioural responsiveness during drowsiness. Brain Topogr. 32, 315–331.
Corradini, P.L., Persinger, M.A., 2014. Spectral power, source localization and microstates to quantify chronic deficits from 'mild' closed head injury: correlation with classic neuropsychological tests. Brain Inj. 28, 1317–1327.
Cortes, C., Vapnik, V., 1995. Support-vector networks. Mach. Learn..
Custo, A., Van De Ville, D., Wells, W.M., Tomescu, M.I., Brunet, D., Michel, C.M., 2017. Electroencephalographic resting-state networks: source localization of microstates. Brain Connect. 7, 671–682.
Denis, Brunet, Micah, M., Murray, Christoph, M., Michel, 2011. Spatiotemporal analysis of multichannel EEG: CARTOOL. Comput. Intell. Neurosci. 2011, 813870.
Drissi, N.M., Szakacs, A., Witt, S.T., Wretman, A., Ulander, M., Stahlbrandt, H., Darin, N., Hallbook, T., Landtblom, A.M., Engstrom, M., 2016. Altered brain microstate dynamics in adolescents with narcolepsy. Front. Hum. Neurosci. 10, 369.
Fitzgerald, P.J., Watson, B.O., 2018. Gamma oscillations as a biomarker for major depression: an emerging topic. Transl. Psychiatry 8, 177.
Grieder, M., Koenig, T., Kinoshita, T., Utsunomiya, K., Wahlund, L.O., Dierks, T., Nishida, K., 2016. Discovering EEG resting state alterations of semantic dementia. Clin. Neurophysiol. 127, 2175–2181.
Gschwind, M., Hardmeier, M., Van De Ville, D., Tomescu, M.I., Penner, I.K., Naegelin, Y., Fuhr, P., Michel, C.M., Seeck, M., 2016. Fluctuations of spontaneous EEG topographies predict disease state in relapsing-remitting multiple sclerosis. Neuroimage Clin. 12, 466–477.
Gudmundsson, S., Runarsson, T.P., Sigurdsson, S., Eiriksdottir, G., Johnsen, K., 2007. Reliability of quantitative EEG features. Clin. Neurophysiol. 118, 2162–2171.
Ip, C.T., Ganz, M., Ozenne, B., Sluth, L.B., Gram, M., Viardot, G., l'Hostis, P., Danjou, P., Knudsen, G.M., Christensen, S.R., 2018. Pre-intervention test-retest reliability of EEG and ERP over four recording intervals. Int. J. Psychophysiol. 134, 30–43.
Katayama, H., Gianotti, L.R., Isotani, T., Faber, P.L., Sasada, K., Kinoshita, T., Lehmann, D., 2007. Classes of multichannel EEG microstates in light and deep hypnotic conditions. Brain Topogr. 20, 7–14.
Khanna, A., Pascual-Leone, A., Farzan, F., 2014. Reliability of resting-state microstate features in electroencephalography. PLoS One 9, e114163.
Khanna, A., Pascual-Leone, A., Michel, C.M., Farzan, F., 2015. Microstates in resting-state EEG: current status and future directions. Neurosci. Biobehav. Rev. 49, 105–113.
Kikuchi, M., Koenig, T., Munesue, T., Hanaoka, A., Strik, W., Dierks, T., Koshino, Y., Minabe, Y., 2011. EEG microstate analysis in drug-naive patients with panic disorder. PLoS One 6, e22912.
Kikuchi, M., Koenig, T., Wada, Y., Higashima, M., Koshino, Y., Strik, W., Dierks, T., 2007. Native EEG and treatment effects in neuroleptic-naive schizophrenic patients: time and frequency domain approaches. Schizophr. Res. 97, 163–172.
Laganaro, M., 2017. Inter-study and inter-individual consistency and variability of EEG/ERP microstate sequences in referential word production. Brain Topogr. 30, 785–796.
Lai, W.J.K.T., 1988. A criterion for determining the number of groups in a data set using sum-of-squares clustering. Biometrics 44, 23–34.
Lehmann, D., Faber, P.L., Galderisi, S., Herrmann, W.M., Kinoshita, T., Koukkou, M., Mucci, A., Pascual-Marqui, R.D., Saito, N., Wackermann, J., Winterer, G., Koenig, T., 2005. EEG microstate duration and syntax in acute, medication-naive, first-episode schizophrenia: a multi-center study. Psychiatry Res. 138, 141–156.
Lehmann, D., Ozaki, H., Pal, I., 1987. EEG alpha map series: brain micro-states by space-oriented adaptive segmentation. Electroencephalogr. Clin. Neurophysiol. 67, 271–288.
Li, Y., Shi, W., Liu, Z., Li, J., Wang, G., 2020. Effective brain state estimation during propofol-induced sedation using advanced EEG microstate spectral analysis. IEEE J. Biomed. Health Inform. PP, 1-1.
Michel, C.M., Koenig, T., 2017. EEG microstates as a tool for studying the temporal dynamics of whole-brain neuronal networks: a review. Neuroimage 180, 577–593.
Milz, P., Pascual-Marqui, R.D., Achermann, P., Kochi, K., Faber, P.L., 2017. The EEG microstate topography is predominantly determined by intracortical sources in the alpha band. Neuroimage 162, 353–361.
Mishra, A., Englitz, B., Cohen, M.X., 2020. EEG microstates as a continuous phenomenon. Neuroimage 208, 116454.
Murray, M.M., Brunet, D., Michel, C.M., 2008. Topographic ERP analyses: a step-by-step tutorial review. Brain Topogr. 20, 249–264.
Musso, F., Brinkmeyer, J., Mobascher, A., Warbrick, T., Winterer, G., 2010. Spontaneous brain activity and EEG microstates. A novel EEG/fMRI analysis approach to explore resting-state networks. Neuroimage 52, 1149–1161.
Nishida, K., Morishima, Y., Yoshimura, M., Isotani, T., Irisawa, S., Jann, K., Dierks, T., Strik, W., Kinoshita, T., Koenig, T., 2013. EEG microstates associated with salience and frontoparietal networks in frontotemporal dementia, schizophrenia and Alzheimer's disease. Clin. Neurophysiol. 124, 1106–1114.
Pascual-Marqui, R.D., Michel, C.M., Lehmann, D., 1995. Segmentation of brain electrical activity into microstates: model estimation and validation. IEEE Trans. Biomed. Eng. 42, 658–665.
Seitzman, B.A., Abell, M., Bartley, S.C., Erickson, M.A., Bolbecker, A.R., Hetrick, W.P., 2017. Cognitive manipulation of brain electric microstates. Neuroimage 146, 533–543.
Sharmila, A., 2018. Epilepsy detection from EEG signals: a review. J. Med. Eng. Technol. 42, 368–380.
Shi, W., Li, Y., Liu, Z., Li, J., Wang, Q., Yan, X., Wang, G., 2020. Non-canonical microstate becomes salient in high density EEG during propofol-induced altered states of consciousness. Int. J. Neural Syst. 30, 2050005.
Shoukri, M.M., Colak, D., Kaya, N., Donner, A., 2008. Comparison of two dependent within subject coefficients of variation to evaluate the reproducibility of measurement devices. BMC Med. Res. Methodol. 8, 24.
Shrout, P.E., Fleiss, J.L., 1979. Intraclass correlations: uses in assessing rater reliability. Psychol. Bull. 86, 420–428.
Skrandies, W., 1990. Global field power and topographic similarity. Brain Topogr. 3, 137–141.
Strelets, V., Faber, P.L., Golikova, J., Novototsky-Vlasov, V., Koenig, T., Gianotti, L.R.R., Gruzelier, J.H., Lehmann, D., 2003. Chronic schizophrenics with positive symptomatology have shortened EEG microstate durations. Clin. Neurophysiol. 114, 2043–2051.
Strik, W.K., Dierks, T., Becker, T., Lehmann, D., 1995. Larger topographical variance and decreased duration of brain electric microstates in depression. J. Neural Trans. Gen. Sect. 99, 213–222.
Tomescu, M.I., Rihs, T.A., Roinishvili, M., Karahanoglu, F.I., Schneider, M., Menghetti, S., Van De Ville, D., Brand, A., Chkonia, E., Eliez, S., Herzog, M.H., Michel, C.M., Cappe, C., 2015. Schizophrenia patients and 22q11.2 deletion syndrome adolescents at risk express the same deviant patterns of resting state EEG microstates: a candidate endophenotype of schizophrenia. Schizophr. Res. Cogn. 2, 159–165.
von Wegner, F., Knaut, P., Laufs, H., 2018. EEG microstate sequences from different clustering algorithms are information-theoretically invariant. Front. Comput. Neurosci. 12.
von Wegner, F., Tagliazucchi, E., Laufs, H., 2017. Information-theoretical analysis of resting state EEG microstate sequences - non-Markovianity, non-stationarity and periodicities. Neuroimage 158, 99–111.
Wang, G., Liu, Z., Feng, Y., Li, J., Yan, X., 2019. Monitoring the depth of anesthesia through the use of cerebral hemodynamic measurements based on sample entropy algorithm. IEEE Trans. Bio-med. Eng. PP.
Wang, H., Wang, Y., Zhang, Y., Dong, Z., Huang, L., 2021. Differentiating propofol-induced altered states of consciousness using features of EEG microstates. Biomed. Signal Process. Control 64, 102316.
Zappasodi, F., Croce, P., Giordani, A., Assenza, G., Giannantoni, N.M., Profice, P., Granata, G., Rossini, P.M., Tecchio, F., 2017. Prognostic value of EEG microstates in acute stroke. Brain Topogr. 30, 698–710.